EUROPEAN ORGANIZATION FOR NUCLEAR RESEARCH

AD/afm CERN/PS/87-13 (AA)

ANTIPROTON - POSITIVE ION TRANSVERSE INSTABILITIES IN THE CERN ANTIPROTON ACCUMULATOR. A TUNE MODULATED DIRECT MAP SIMULATION.

A. Dainelli

Abstract

A direct map method with a Mathieu approach on tune modulation is used to simulate non-linear effects on particle motion which are generated by a beam-beam like interaction of antiprotons with ions of the residual gas in the CERN Antiproton Accumulator. Two different ion distributions are used and the behaviour of particle motion is studied in phase space with particular attention to high-order non-linear resonances.

Geneva, Switzerland

February 1987

CONTENTS

1. INTRODUCTION

In circular accelerators or storage rings, with negative beams (antiprotons or electrons), positive ions arising from ionisation of residual gas molecules or positive charged microparticles can be trapped by the negative potential generated by the beam itself. If the efficiency of clearing devices is not very good, the ions of the residual gas will continue to accumulate until an equilibrium neutralisation of about 0.998 is reached. The efficiency of clearing electrodes is different for different places of the storage ring because of different geometries (chamber enlargements, special tanks, etc.); therefore pockets of ions are localised in few regions of the ring where clearing action is more difficult. When the intensity of the stacked beam becomes important, the interactions of the beam negative particles with the positive matter (ions or microparticles) can produce a systematic increase in transverse emittances. With the CERN Antiproton Accumulator (AA) a stack intensity above 10^{11} antiprotons and transverse emittances between π and 2π mm.mrad (at 3.5 GeV/c) are sufficient to exhibit abnormal growth of transverse emittances that can be related to the mechanism described above[1]. The average gauge pressure of the AA during normal operation is about 10^{-11} torr with 90% H_2 and 10% of CO or N_2 residual gas. With this pressure each antiproton can produce with roughly the same probability an ion of the H_2^+, CO^+ or N_2^+ kind in about 25 seconds (mean time). The neutralisation process, through multiple coulomb scattering, favours the escape of heavy ions (CO^+, N_2^+) and the final ion pocket is therefore mainly populated by protons as a result of double ionisation of molecular hydrogen.

The interaction of antiprotons with the few ion pockets (mainly protons) should be therefore very similar to the beam-beam interaction in colliding beam machines[2]. The electromagnetic field generated by the ion distribution can be described by a transcendent function which in principle contains all the powers of transverse coordinates (x and y). The presence of all powers of transverse coordinates in the perturbing force makes the system highly non-linear and, with the non-definite parity of the distribution, explains the excitation of high-order non-linear resonances. In order to focus the attention on the CERN AA phenomenology Fig. 1 reproduces two pictures from Ref. 1.

The tune diagram of AA can be seen with a scan on horizontal betatron tune which shows the emittance growth due to the crossing of several 15th and 11th order non-linear resonances. To explain the behaviour shown in Fig. 1 some tune modulation (from ripple in the AA magnet current) must be also considered. The estimated tune modulation amplitude is about $\Delta\nu \approx 3 \cdot 10^{-5}$ and its frequency is 300 Hz. The effect described above with others connected to the possible presence of SiO_2 microparticles are potential limitations to the CERN Antiproton Accumulator performance; these limitations can become serious with the higher intensities which will be possible after the completion of the ACOL project[3] in 1987. A good understanding of non-linear problems in the AA seems therefore quite profitable.

Furthermore, the AA phenomenology, as described above, seems also to be an interesting application field for many of the general ideas on non-linear dynamics such as non-linear maps, instability, phase space structure and chaos from deterministic motion. If we describe the particle motion in a storage ring using the azimuthal coordinate s as the independent variable, directly proportional to the time, and focus the attention on transverse motion, the system has only two degrees of freedom (the Hamiltonian is supposed to

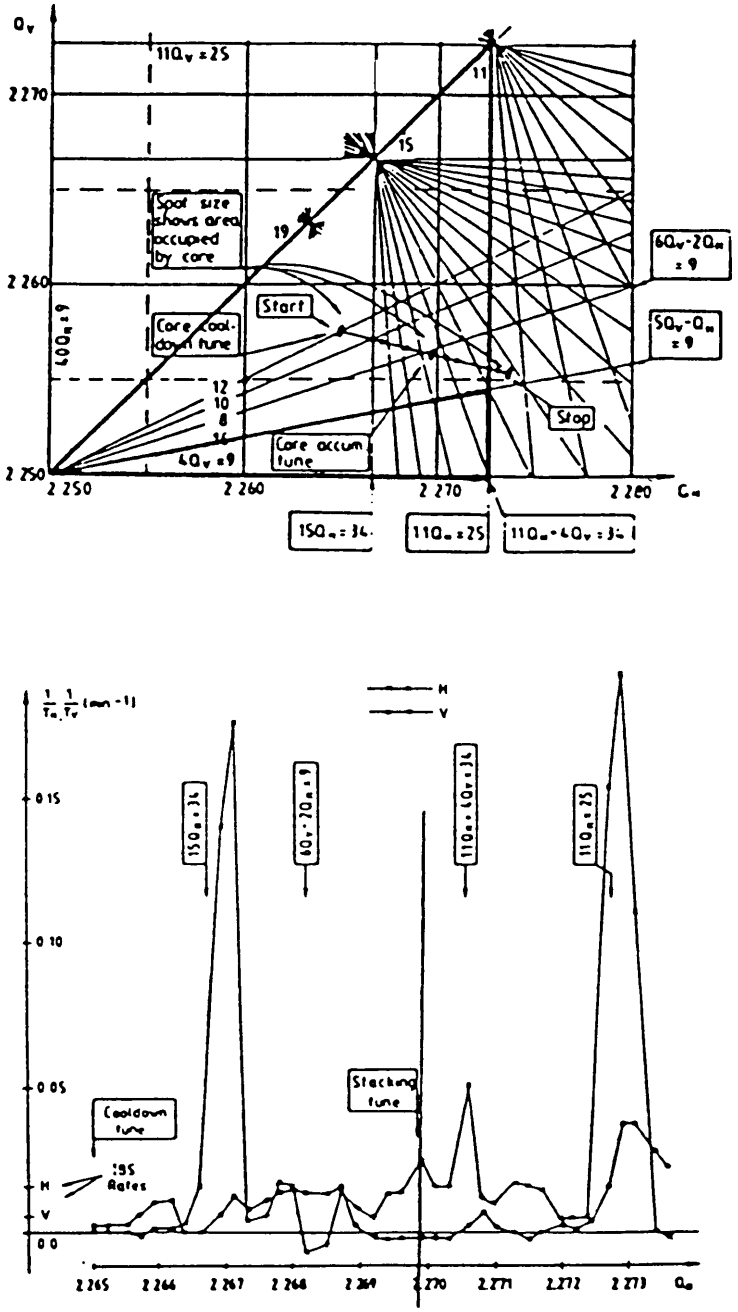

Fig. 1 - a) Tune diagram of the CERN Antiproton Accumulator and b) Growth of the emittances during a scan of horizontal betatron tune (from Ref. 1).

be independent of s) and the phase-space behaviour can be visualised without too much difficulty. Indeed, with two degrees of freedom, the phase space, where the motion can be represented, is a four-dimensional manifold and a surface of constant energy is a three-dimensional space in which a dense set of bidimensional nested tori defines the surfaces of invariant linear motion[4]. Each torus is associated with a value of the constant of motion (the amplitude in this case) which spans the constant-energy "surface" (the three-dimensional volume). Finally, with the time evolution, the representative point of the motion in phase space moves always upon the invariant torus which is defined by the initial

amplitude. The phase-space plots of the motion, or the map development, can therefore be thought as the signature of the representative point as this crosses a plane in phase space (x-p_x, y-p_y or x-y). As a small non-linear perturbation (such as the antiproton-ion interaction in the AA) is added to the linear system described above, the phase-space pattern becomes more complicated and the motion can become unstable. The aim of this note is just to study in a detailed way the behaviour of the phase space and the occurrence of non-linear resonances in a linear system (the linear betatron motion of charged particles in storage rings) upon which a weak non-linear perturbation (the antiproton-ion interaction) is added.

2. *DIRECT MAP FORMALISM*

A rudimentary description of charged particle transverse motion in circular machines can be the simple harmonic oscillator; in this description every local (fine) peculiarity of the ring lattice is neglected and only the overall sinusoidal pattern is taken into account. In this picture the harmonic oscillator equations can be the starting point for a subsequent analysis in which further aspects of charge particle motion such as tune modulation (due to ripple in magnet currents or synchrotron oscillations) and periodic interactions (beam-beam like) between antiprotons and positive particles can be studied in a direct way. If x and y are coordinates in space transverse to particle trajectory and θ is the azimuthal coordinate, ν_x and ν_y the corresponding betatron tunes, the uncoupled harmonic oscillator description is:

$$\begin{aligned} x''(\theta) + \nu_x^2\, x(\theta) &= 0 \\ y''(\theta) + \nu_y^2\, y(\theta) &= 0 \ . \end{aligned} \tag{1}$$

The same two equations of motion can be of course derived from a classical Hamiltonian approach[5]. Tune modulation and periodic kicks can then be introduced in equations (1):

$$x''(\theta) + \nu_{0x}^2(1 - \lambda \cos\nu_s\theta)x(\theta) = \xi x \Phi(x,y) \sum_n \delta(\theta - n2\pi) \ . \tag{2}$$

Two types of interactions contribute to the slope variation x'' in equation (2); the first one is the restoring force of the "rudimentary" lattice (slightly modulated) while the second one, active in a single point of the ring (and so at every multiple of 2π in θ) is an instantaneous kick whose strength is determined by a coupling constant ξ and by the impact point (x,y) by means of the localised ion pocket distribution described by the Φ function which is non-linear in x and y coordinates. A more detailed description of the ξ coupling constant and of the Φ function in terms of electrostatic forces is given below (par. 3). Equation (2) without the right member is a classical Mathieu equation which, in order to follow classical textbooks on mathematical functions, can be rewritten by means of the new variable $z = \nu_s\theta/2$:

$$x''(z) + (a - 2q\cos 2z)x(z) = (2/\nu_s)\xi x \Phi(x,y) \sum_n \delta(z - n\pi\nu_s) \tag{3}$$

with $a = 4(\nu_x/\nu_s)^2$ and $q = 2(\nu_x/\nu_s)^2\lambda$; if $q \ll 1$, classical solutions of Mathieu equation

are the elliptical sine and cosine M(z) and N(z) (see Appendix A). The physical system is completely determined by equation (2) or (3). To obtain a useful numerical tool to follow the behaviour of a particle in this system, we can derive a direct map from equation (3) which can give the phase-space coordinates of the particle at the $(n + 1)^{-th}$ turn by means of the phase-space coordinates at tne n^{-th} turn[6-7].

In free zones (free from kicks) equation (3) becomes a homogeneous Mathieu equation and therefore the general solution is a linear superposition of elliptical sine and elliptical cosine (or their Liouville's transform[8]; see Appendix A):

$$x(z) = A\,M(z) + B\,N(z)$$

where A and B are constants which are determined by the initial conditions after the last kick. Coefficients A and B are then peculiar to each "free zone"; so, solutions in each "free zone" are:

$$\begin{aligned} x_n &= A_n\,M(z) + B_n\,N(z) \\ x_n' &= A_n\,M'(z) + B_n\,N'(z) \end{aligned} \tag{4}$$

To complete the description the kick which determines A_n and B_n must be added. This can be accomplished by integrating equation (3) and neglecting the restoring force of the lattice:

$$\begin{aligned} \int x''\,dz &= (2/v_s)\xi \int x\Phi \sum\delta(z - n\pi v_s)\,dz \\ x_{n+1}'(n\pi v_s + \varepsilon) - x_n'(n\pi v_s - \varepsilon) &= (2/v_s)\xi\, x_n(n\pi v_s)\Phi(n) \end{aligned} \tag{5}$$

The direct map can be obtained from equation (5) plus the request of continuity of the solution at the kick point ($x_{n+1}(n\pi v_s) = x_n(n\pi v_s)$):

$$\begin{aligned} A_{n+1}\,M(n) + B_{n+1}\,N(n) &= x_n(n\pi v_s) \\ A_{n+1}\,M'(n) + B_{n+1}\,N'(n) &= x_n'(n\pi v_s) + (2/v_s)\xi x_n(n\pi v_s)\Phi(n) \end{aligned} \tag{6}$$

The system of equations (6) determines completely the values of A_{n+1} and B_{n+1} by means of the phase-space coordinate n^{-th} turn values $x_n(n)$ and $x_n'(n)$.

$$\begin{aligned} A_{n+1} &= [x_n(n)N'(n) - \alpha(n)N(n)]/\Delta \\ B_{n+1} &= [\alpha(n)M(n) - x_n(n)M'(n)]/\Delta \end{aligned} \tag{6a}$$

with the following definitions for Δ and $\alpha(n)$:

$$\Delta = M(n)N'(n) - M'(n)N(n)$$

$$\alpha(n) = x'_n(h) + (2/v_s)\xi_n(n)\Phi(n)$$

The recursive relationship between x_{n+1} and x_n (or x'_{n+1} and x_n), the Direct Map, can be obtained from the general solution x_{n+1} evaluated at $z = (n + 1)\pi v_s$ with the expressions given in (6a) for A_{n+1} and B_{n+1}:

$$\begin{aligned} x_{n+1}(n + 1) &= A_{n+1}\, M(n + 1) + B_{n+1}\, N(n + 1) \\ x'_{n+1}(n + 1) &= A_{n+1}\, M'(n + 1) + B_{n+1}\, N'(n + 1) \end{aligned} \tag{7}$$

The final expression for the Map becomes:

$$\begin{aligned} x_{n+1}(n + 1) &= [D_1 x_n(n) + D_2(x'_n(n) + (2/v_s))\xi x_n(n)\Phi(n)]/D \\ x'_{n+1}(n + 1) &= [D_3 x_n(n) + D_4(x'_n(n) + (2/v_s))\xi x_n(n)\Phi(n)]/D \end{aligned} \tag{8}$$

with

$D = -\Delta = M'(n)N(n) - M(n)N'(n)$,
$D_1 = M'(n)N(n + 1) - M(n + 1)N'(n)$,
$D_2 = M(n + 1)N(n) - M(n)N(n + 1)$,
$D_3 = M'(n)N'(n + 1) - M'(n + 1)N'(n)$,
$D_4 = M'(n + 1)N(n) - M(n)N'(n + 1)$.

3. FORCES ACTING ON ANTIPROTONS

Space charge forces acting on antiprotons can be derived from Gauss' theorem, and Ampere's law[2]; with a cylindrical charge distribution we obtain:

$$F_{sc}(r) = (n\, e^2/2\pi\varepsilon_0)(1 - \beta^2)\, D(r)/r\ . \tag{9}$$

n is the linear antiproton density in the beam and $\beta = v/c$; D(r) depends on the chosen beam distribution and is equal to:

$$D(r) = 1 - \exp(-r^2/2\sigma^2) \tag{10}$$

with

$$\varrho(r) = (ne/2\pi\sigma^2)\, \exp(-r^2/2\sigma^2)\ . \tag{11}$$

With the antiproton γ value in the CERN Antiproton Accumulator ($\gamma = 3.77$), the space charge force drops to about 7% of the electrostatic force.

When the antiprotons travel through an ion cloud somewhere in the AA ring, the radial force acting on them can be described by (again with cylindrical symmetry):

$$F_{ions}(r) = -\eta(n\, e^2/2\pi\varepsilon_0)(1 + \beta^2)\, D(r^2/2\sigma^2)/r \tag{12}$$

in which η is the neutralisation factor in the ion cloud, $n_{ions} = \eta n$ (the mean value all around the ring is of the order of 20%); the x and y components of this radial force are:

$$F_x = -(x/r)\left|F_{ions}(r)\right| = -\eta(ne^2/2\pi\varepsilon_0)(1 + \beta^2)\ x\ D(r^2/2\sigma^2)/r^2 \qquad (13)$$

$$F_y = -(y/r)\left|F_{ions}(r)\right| = -\eta(ne^2/2\pi\varepsilon_0)(1 + \beta^2)\ y\ D(r^2/2\sigma^2)/r^2\ . \qquad (14)$$

For the slope deviation we can write:

$$x'(\theta) = (R/\omega p)F_x\ , \qquad y'(\theta) = (R/\omega p)F_y\ , \qquad (15)$$

ω is the revolution frequency and p the reference momentum; for the x direction we have:

$$x'(\theta) = -(R/\omega p)\ \eta\ (n\ e^2/2\pi\varepsilon_0)(1 + \beta^2)\ x\ D(r^2/\sigma^2)/r^2 \qquad (16)$$

$$x'(\theta) = -(n\ r_p/\gamma 2\sigma^2)(Rc/\omega)((1 + \beta^2)/\beta)\ \eta\ x\ D(r^2/\sigma^2)/(r^2/2\sigma^2)\ . \qquad (17)$$

If we suppose that the change in slope is made abruptly at $\theta = k2\pi$, we can write:

$$\Delta(x') = -(Nr_p/2\gamma\sigma^2)((1 + \beta^2)/\beta)\ R\eta\ x\Phi(r^2/2\sigma^2)(L/R) \sum_k \delta(\theta - k2\pi)\ . \qquad (18)$$

$N = \int n(s)\ ds = nL$ and $\Delta\theta = L/R$ have been introduced because of dimensional considerations. We can define a coupling constant ξ and rewrite:

$$\Delta(x') = \xi x\Phi(r^2/2\sigma^2) \sum_k \delta(\theta - k2\pi) \qquad (19)$$

$$\xi = -(N\ r_p/2\gamma\sigma^2)((1 + \beta^2)/\beta)\ \eta L\ . \qquad (20)$$

The change in slope $x'(\theta)$ at each $\theta = k2\pi$ is therefore:

$$\Delta(x') = \xi\ x\ \Phi(r^2/2\sigma^2)\ . \qquad (21)$$

With $\sigma = 1$ mm, $r_p = 1.5 \cdot 10^{-18}$ m, $N = 0.2 \cdot 10^{10}$ $\bar{p}$/m and L = 1 m, realistic values of the coupling constant come out to be of the order of $10^{-3} \div 10^{-2}$; in this range the result is strongly dependent on the L and η values.

A more realistic distribution with still a gaussian shape but $\sigma_x \neq \sigma_y$ ($\sigma_x > \sigma_y$) is:

$$\varrho(x,y) = (ne^2/2\pi\sigma_x\sigma_y)\ \exp(-x^2/2\sigma_x^2 - y^2/\sigma_{y2})\ . \qquad (22)$$

With this "elliptical" distribution the slope deviation can be written as[9]:

$$\Delta(x') = \xi^* Im\{W(z)\}\ , \qquad \Delta(y') = \xi^* Re\{W(z)\} \qquad (23)$$

with

$$\xi^* = \xi(\sqrt{\pi/2})\sigma^2/(\sigma_x^2 - \sigma_y^2)\ . \qquad (24)$$

$$W(z) = (1/\kappa)\{w((x + iy)\kappa) - \exp[-(x/2\sigma_x)^2 + (y/2\sigma_y)^2]\ w((xr + iy)/r)\kappa\} \qquad (25)$$

$$\kappa = 1/\sqrt{2(\sigma_x^2 - \sigma_y^2)} \qquad (26)$$

w(z) is the complex error function defined as[10]:

$$w(z) = e^{-z^2}[1 + (2i/\sqrt{\pi}) \int^{z} e^{\zeta^2} d\zeta \qquad (27)$$

and can be evaluated by means of a fast computer program[11] which can be very useful in particle tracking simulations and is available from the CERN program library.

4. NUMERICAL SIMULATIONS

4.1 Summary of Qualitative Features of Weakly Perturbed Systems

The uncoupled linear motion described by equations (1) can be represented in phase space by the product of two independent ellipses, i.e. a torus upon which the representative point moves with the time evolution. From a more formal point of view, a system with two degrees of freedom can be integrated if one can find two integrals of the motion which are independent (Liouville's theorem). For the uncoupled harmonic oscillators energy and amplitudes are constants of the motion; because of the constant energy, the motion in phase space (4-dimensional) is confined to a "surface" (a volume) of constant energy; the invariant amplitude confines furthermore the motion to a surface of constant amplitude: the torus.

The motion of the representative point upon the torus can be described by two coordinates, θ_1 and θ_2; the former coordinate is the polar coordinate on the torus cross section while the latter is just the azimuthal coordinate around the torus. If $\omega_1 = \theta_1$ and $\omega_2 = \theta_2$ are in a rational relationship ($m\omega_1 = n\omega_2$; m and n integers), the representative point of the motion closes its orbit after m revolutions upon the torus; the signatures that it leaves through a plane in phase space during the first m turns are also the crossing points of the successive motion. The invariant torus is said to be rational. If ω_1 and ω_2 are not in a rational relationship the orbit remains open for ever, the trajectory of the representative point covers in a dense fashion all the torus surface, and the signature left through a plane during the motion is a continuous curve (ellipse). The invariant torus is said to be irrational.

The ratio ω_1/ω_2 (winding number) depends on the amplitude of the motion and therefore in general it is different for distinct tori. Thus, if the system is linear and not perturbed the Hamiltonian generates, in phase space projections, invariant curves (dotted or continuous "circles") which belong to rational or irrational winding numbers.

As a small perturbation is added to the linear motion the whole picture becomes extremely complicated; but, if the perturbation is sufficiently weak, tori with irrational winding number survive although in a distorted form. On the other hand, tori with rational winding numbers are completely destroyed and the pattern of phase-space projections looks like small circles around stable fixed points separated by diffuse regions with an unstable fixed point at each of them. These unstable fixed points are at the origin of the deterministic chaotic motion in phase space, i.e. motion which is extremely sensitive to the initial condition. Typical behaviours as described above can be seen in the following sections (Figs. 7 and 11).

4.2 Non-linear Resonances

A numerical code (DIRMAP) has been derived from the Direct Map relationship described in equation (8) (the M and N functions are the Mathieu functions or their Liouville's transforms according to the values of the parameters; see Appendix A). This simple numerical tool makes it possible to investigate some interesting aspects of charged particles behaviour in a storage ring in the presence of non-linear forces such as those which originate from the antiproton-positive ion interactions described above. Furthermore, the aspects related to tune modulation can also be investigated because of the peculiar Mathieu approach in DIRMAP (equation (2)).

With two coupled degrees of freedom, non-linear resonances in motion amplitude can be found with values of the transverse betatron tunes ν_x and ν_y which satisfy the well known resonant condition:

$$m\nu_x + n\nu_y = p \tag{28}$$

with m, n, p integers[5,12-13]; $q = |m| + |n|$ is called the order of the non-linear resonance. If some tune modulation with frequency ν_s is active (in both planes) the resonant condition becomes[14-15]:

$$m\nu_x + n\nu_y = p + k\nu_s \ . \tag{29}$$

With tune modulation in one degree of freedom (two-dimensional phase space) each main resonance of order n has an infinite number of satellite resonances which are separated by ν_s/n and reduced in strength by a factor $J_k(n\nu/\nu_s)$, the value of the first kind Bessel function with argument equal to the ratio of n times the modulation amplitude ν to the modulation frequency ν_s[2,12]; the resonant condition becomes:

$$\nu_x = p/n + k\ \nu_s/n \qquad (k = 0, \pm1, \pm2, \ldots) \tag{30}$$

4.3 Third-Integer Resonances Driven by a Sextupolar Field

In order to test confidence in the code, many numerical simulations have been done around a third-integer resonance ($\nu_s = 7/3$) driven by a sextupolar term in the force of the type $x^2 - y^2$ and xy. A typical result obtained with the DIRMAP code is shown in Fig. 2. The horizontal betatron tune is incremented by fixed steps. For each horizontal betatron tune value a sequence of 5000 map iterations is initiated. The iteration is truncated if the particle amplitude becomes greater than a fixed one (related to the physical aperture of the storage ring) and the particle itself can be considered as lost. Two of the outputs of the DIRMAP code consist of tune values of the step and the number of iterations for which the particle survives ($N < 5000$). In Fig. 2 we have plotted the reciprocal of N as a measure of the growth rate; furthermore, the strength has been normalized to be the unity on the exact resonance value ($\nu_x = 7/3$). The first satellite resonance described above is clearly seen at the expected value of horizontal betatron tune ($\nu_x = 2.333 + 0.0780/3 = 2.3593$).

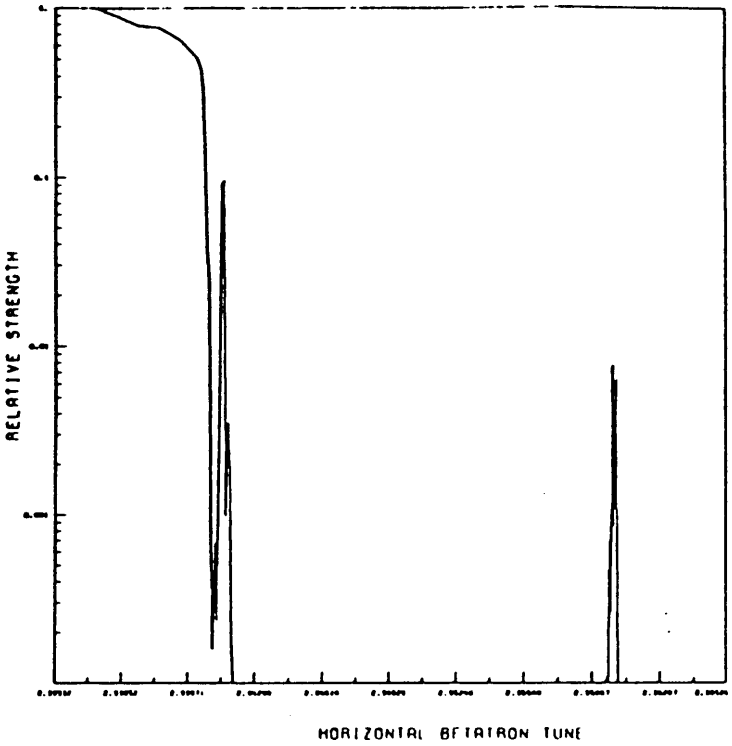

Fig. 2 - Satellite resonance near a third-integer one

The phase space behaviour with the value of the horizontal betatron tune ν_x in the middle of the satellite resonance is shown in Fig. 3 (tune modulation switched off) and Fig. 4 (tune modulation switched on); when the tune modulation is switched off the motion is stable and remains finite as one can see in Fig. 3a; Fig. 3b shows the corresponding development of the J_x which in a linear case would be a constant equal to half the invariant emittance.

Without tune modulation (modulation amplitude set to zero; AM = 0.0) the J_x behaviour although not constant because of non-linear terms, remains finite over at least 5000 turns. With tune modulation switched on, the satellite resonance is present, the phase space plot becomes diffuse and apparently disordered (Fig. 4a); finally, the development of J_x (Fig. 4b) shows sporadic growth with increasing peak value which can be taken as a signature of chaotic motion; the particle is definitely "lost" after about 3500 turns.

Figure 3 suggests that fixed points of the map are located at 0, $2\pi/3$ and $4\pi/3$ radians in phase space. Further simulations have been done to investigate how satellite resonance width depends on the initial phase of motion; results are shown in Fig. 5. Without coupling between the two planes the behaviour of the map with initial phase of $2\pi/3$ rad should be quite similar to the one with an initial phase equal to zero; as the betatron tune moves away from the third integer resonance, the radial dimension of the separatrix in phase space (a well known triangle) becomes greater and greater and a stable region centred at the origin begins to appear. Because of the shape and orientation of the separatrix, portions of phase space centred at fixed radius and with a $2\pi/3$ phase difference should become stable together (at approximately the same values of hte horizontal betatron tune, as this latter is increased). Figure 5 shows that the coupling between the

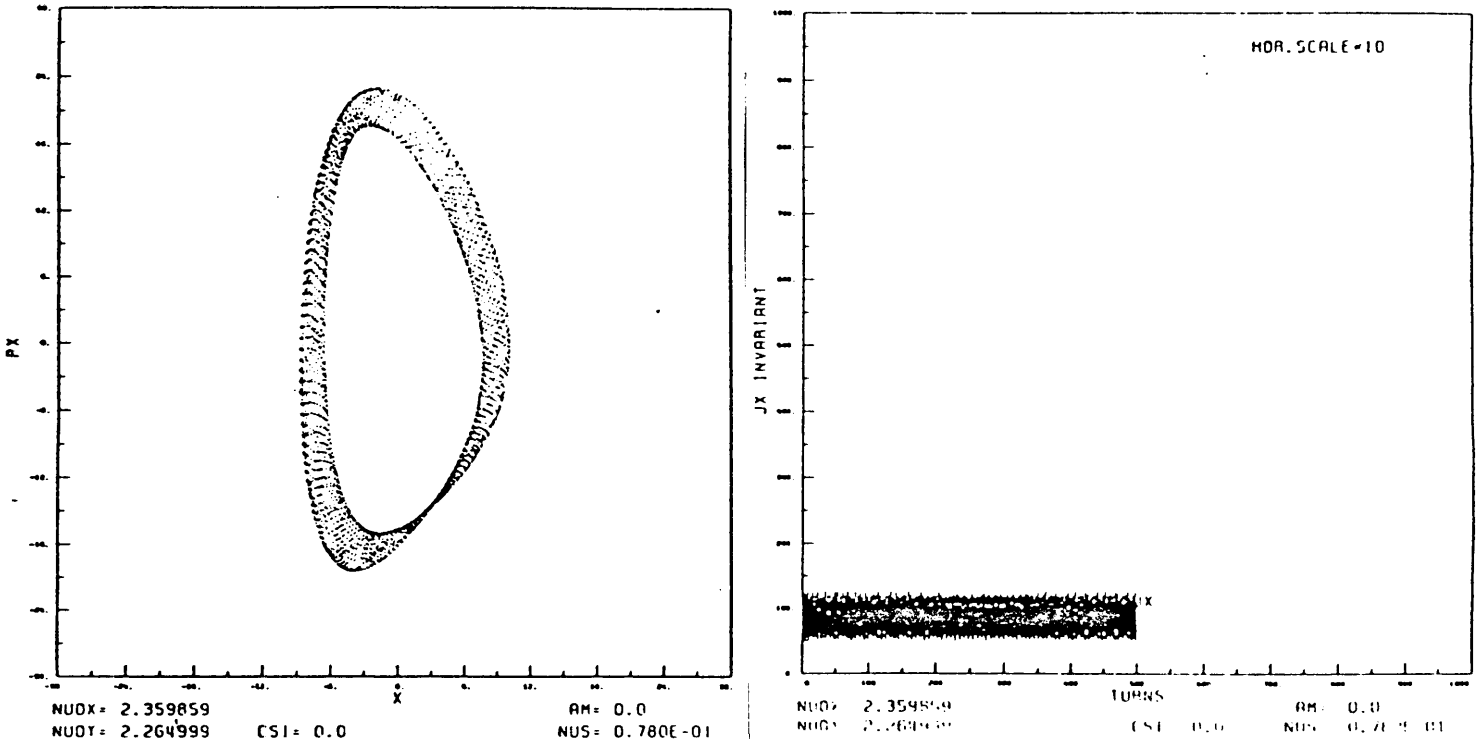

Fig. 3 - Phase space plots and J_x behaviour for a satellite resonance without tune modulation

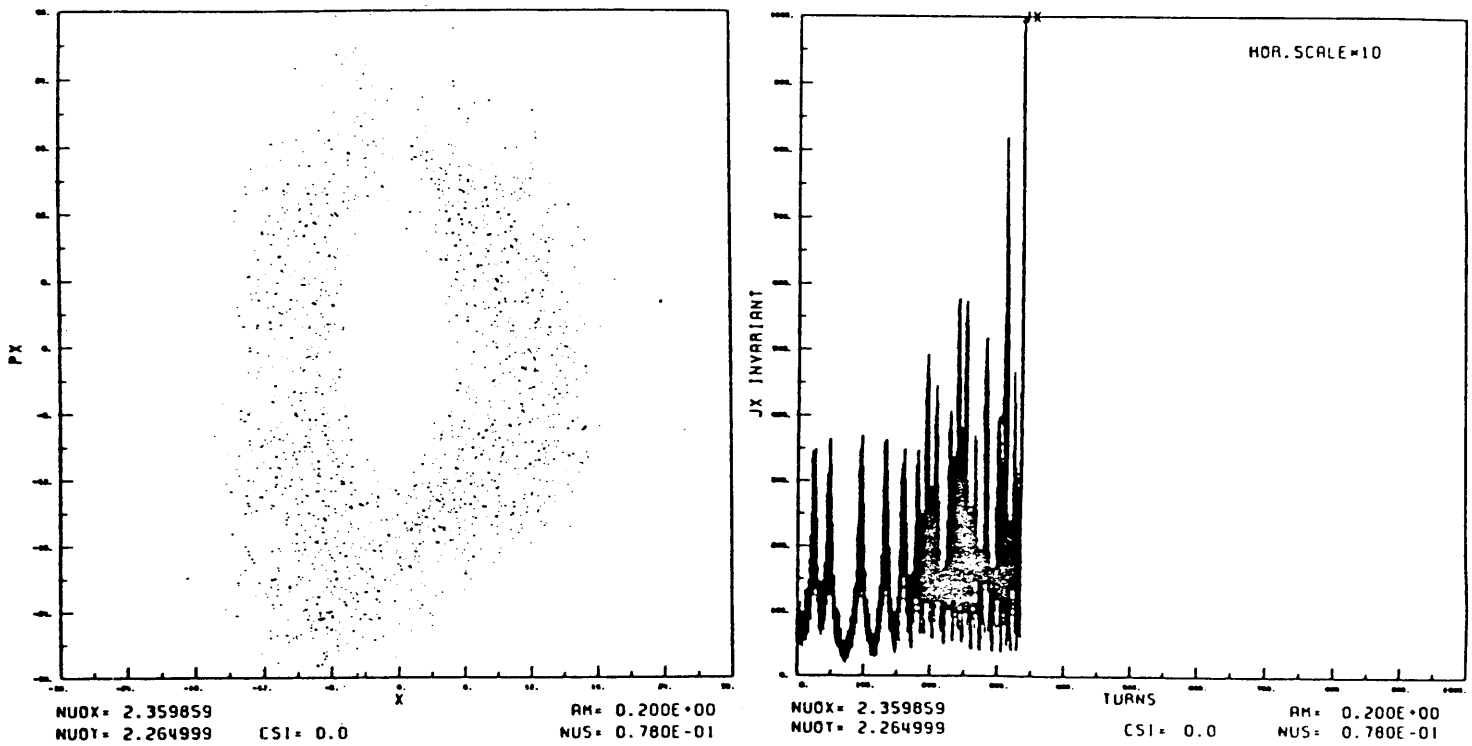

Fig. 4 - Phase space plots and J_x behaviour for a satellite resonance with tune modulation

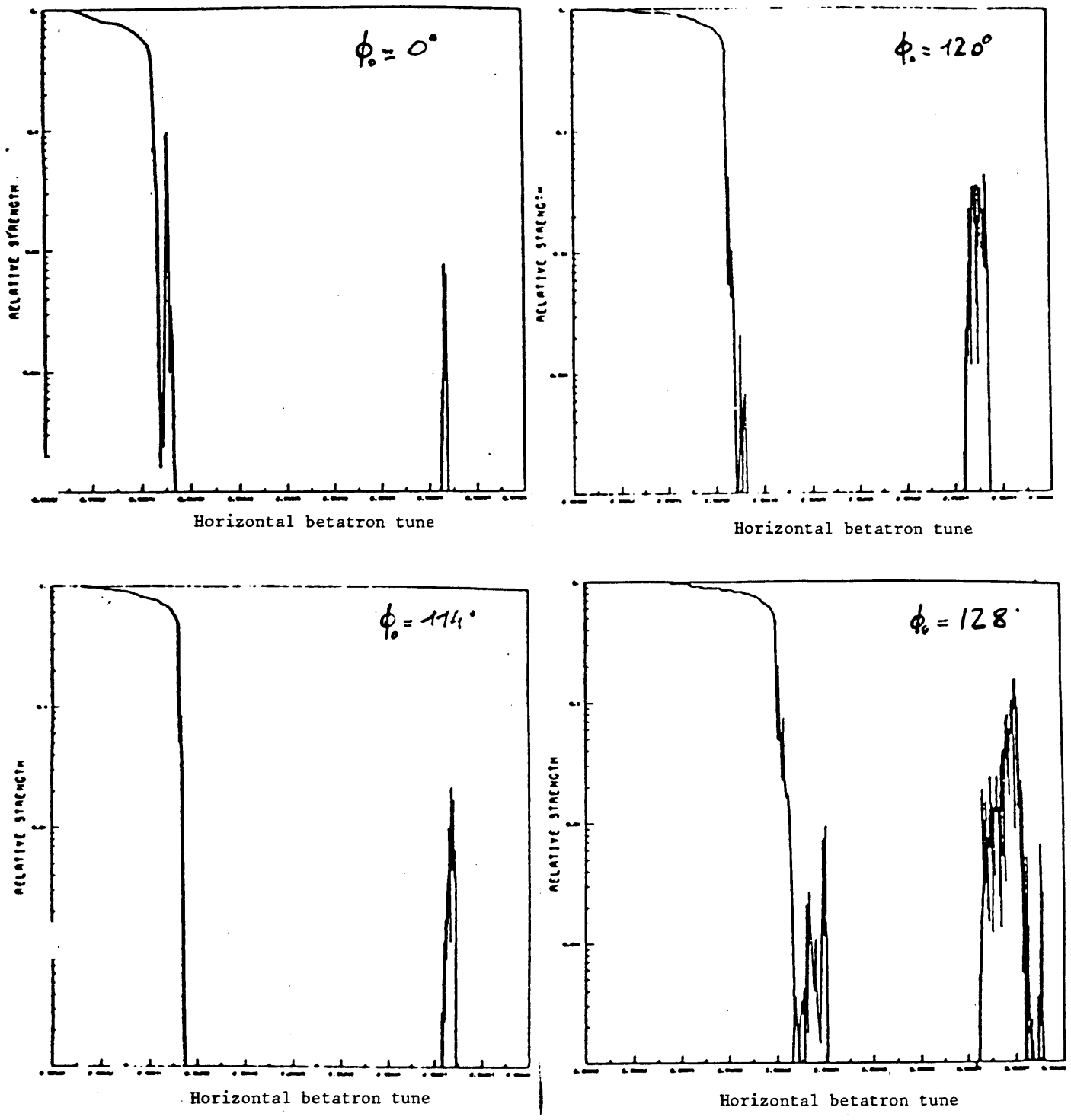

Fig. 5 - Satellite resonance behaviour with different initial phases.

two planes distorts a little the picture described above and a major similarity can be seen in pictures which refer to initial phase of zero and 114 degrees; furthermore, the satellite resonance width seems always related in a direct fashion to the main resonance width without any correlation to the initial phase, as predicted by considerations reported above on the satellite resonance strength.

4.4 Liapounov Exponent as a Signature of Chaotic Motion

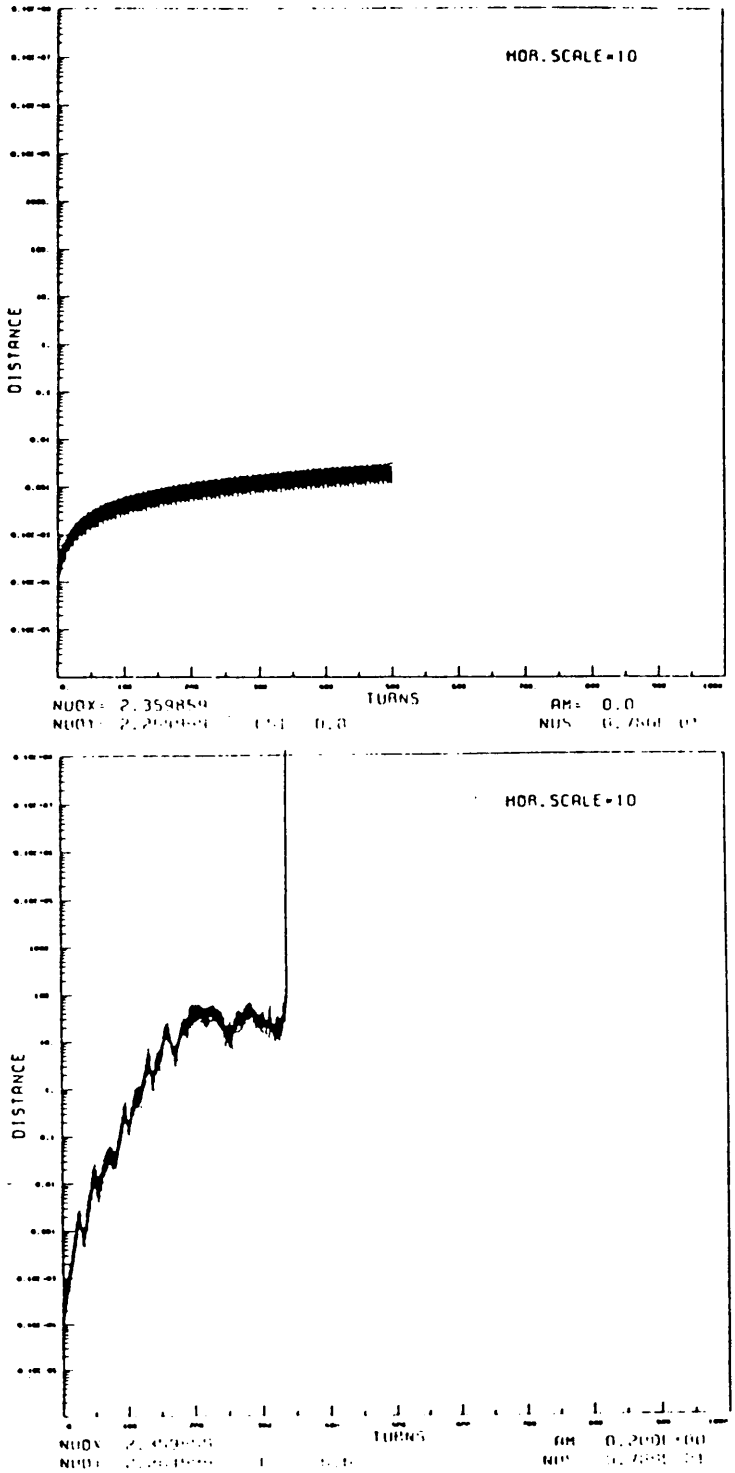

Fig. 6 - Evolution of the distance in phase space for two representative points which are initially close together; signature for regular (a) and chaotic (b) motions.

A more sure signature of chaotic motion is represented by the exponential growth in separation between two representative points which initially have been close together in phase space[15]. The characteristic Liapounov exponent is defined as[16]:

$$\lambda = \lim_{\substack{t\to\infty \\ d(0)\to 0}} \frac{1}{t} \frac{|d(t)|}{|d(0)|} \tag{31}$$

d(t) is the euclidean distance in phase space as a function of time (or turns, or map iterations) and d(0) is the initial euclidean distance of the two representative points. Non-zero Liapounov exponents are a quantitative measure of stochasticity of the motion; if the motion is regular the distance d(t) grows in a linear fashion with time (or turns; $d(N_t) \propto N_t$ and $\lambda = \text{Lim}\, \text{Ln}[N_t/N_t] = 0$). Therefore exponential growth of d(t) indicates chaotic behaviour while linear growth indicates a regular motion. Figure 6 shows the growth of the distance in phase space for two representative points whose initial distance is 10^{-5}. Figure 6a refers to the case in which the tune modulation is switched off (as in Figs. 3a and 3b) and the motion is regular (linear growth with number of turns); Figure 6b refers to the tune modulation switched on (as in Figs. 4a and 4b) and confirms that the motion is chaotic, as deduced above from the area filling feature of Fig. 4a. The saturation value of the distance can be thought of as a measure of the layer of phase space which is available to the motion.

4.5 High-Order Non-Linear Resonances Driven by Gaussian Charge Distributions

Non-linear resonances of high order are in general very difficult to put in evidence by means of simulation codes because of their weakness and consequently the low growth rate of the resonant amplitude. The overall behaviour of the tune modulated complete antiproton-ion potential is better understood if the betatron tune values are chosen near a relatively strong resonance such as a third integer one. Furthermore with this choice, comparisons are possible with the case in which only quadratic terms are present in the force expression (sextupole) as in Fig. 3. Also, the minimum value of the coupling constant, ξ, which is necessary to make active at least the first expansion polynomial terms of the complete gaussian distribution can be better determined near a third-integer resonance.

In order to realise the program described above, the even parity of the charge distribution must be destroyed at least in the x direction if we want to reproduce the odd resonances. This can be easily done by introducing a displacement x_c along the x direction. In this way all the powers of x are present in the $\Phi(x,y)$ expansion and therefore quadratic terms (x^2-y^2, xy) appear in the kick expression as is necessary in order to excite third-integer resonances.

Results obtained with the cylindrical charge distribution and even parity in both x and y directions are presented in Fig. 7 where six different pictures in phase space with increasing ξ values are shown. As ξ increases, more and more non-linear terms of the distribution become important for the dynamical evolution (or map iteration. The first five pictures of Fig. 7 refer to a fixed initial value of the amplitude in both planes ($x-p_x$, $y-p_y$) while the last one, in order to give an idea of the complex structure of the phase space, describes the motion with different initial amplitudes in the $x-p_x$ plane (the $y-p_y$ initial amplitude and phase are kept constant). Furthermore, the last picture of Fig. 7 is a clear example of a classical break of phase space in rational and irrational tori.

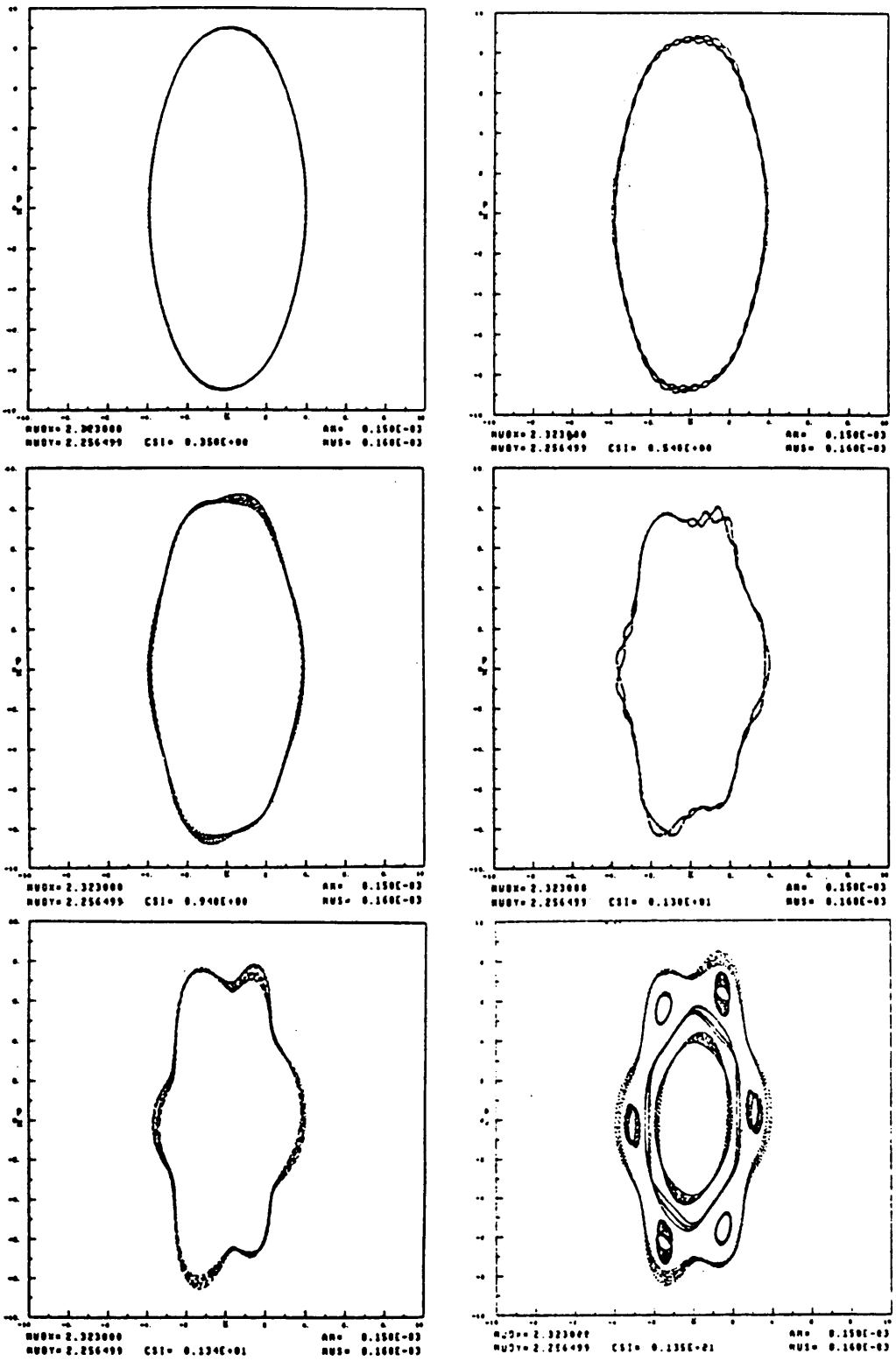

Fig. 7 - Phase-space behaviour of the map with a gaussian distribution and a cylindrical symmetry.

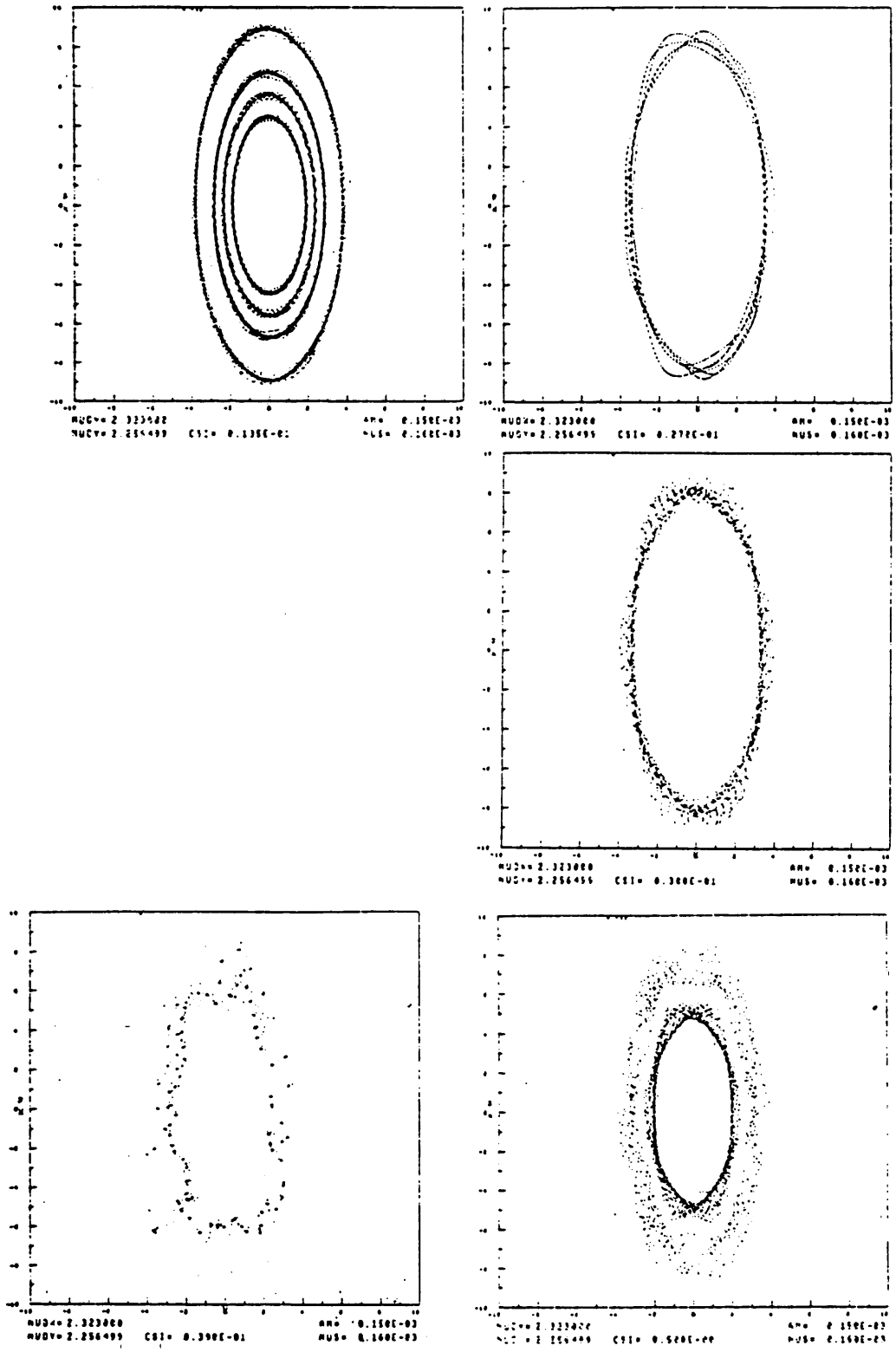

Fig. 8 - Phase-space behaviour of the map with a gaussian charge distribution ($\sigma_x > \sigma_y$)

Although phase space puts in evidence the effect of multipolar terms with the ε value, as long as the even parity is preserved the motion remains regular and finite at least for initial values of phase space coordinates which have a physical meaning.

The first striking difference between cylindrical and elliptical charge distributions is that this latter seems to be more effective to produce unstable motion than the first one. If one tries to use in elliptical distribution values of ξ of the order of the unity and the same initial conditions in both planes as in cylindrical distribution, the motion is completely unstable and no more than ten iterations are possible.

The second important difference is that even when apparent stability is present, the overall behaviour of motion with elliptical charge distribution is much more chaotic than with the cylindrical distribution. Furthermore, upon increasing ξ, the transition from stable to unstable motion seems to be quite abrupt, without steps with rational and irrational tori, as in Fig. 7. The phase-space structure seems also to be completely different. The behaviour described above can be seen in Fig. 8 where different phase-space pictures are reported with increasing the ξ value near the same third-integer resonance but without any decentralisation of the charge distribution; note that the ξ value of the first picture is two orders of magnitude smaller than the ξ value of the last case of Fig. 7.

The same completely different behaviour between cylindrical and elliptical charge distributions can be better seen in pictures of resonance relative strength (reciprocal of number of "turns" before the particle is lost) versus horizontal betatron tune.

When the cylindrical charge distribution is used, even with values of the coupling constant ξ much greater than the physical ones, the behaviour of the map remains stable over the most part of the range where some important non-linear resonances of even parity should appear. This stresses once more the relative weakness of the cylindrical charge distribution to excite non-linear resonances. This behaviour is shown in Fig. 9 where the value of tne coupling constant ξ is equal to 2.0 ($\simeq 100\ \xi_{phys}$). Because of the even parity of charge distribution, only even-order resonances can be excited. The strongest even resonance in the chosen range is $\nu_x = 9/4$. With $\xi = 2.0$ the cylindrical distribution reproduces this peak; the same peak can be also attributed to at least two other non-linear resonances:

$$\begin{aligned} 2\nu_x + 2\nu_y &= 9, \qquad \nu_x = 2.2435 \\ 3\nu_x + \nu_y &= 9, \qquad \nu_x = 2.24783 \end{aligned} \tag{31}$$

Three other peaks are reproduced by the cylindrical distribution and their most probable idenditification is given in the picture.

As suggested above, the definite parity (even) of the cylindrical distribution can be destroyed by giving a displacement by a quantity x_c to its centre. In this way also the odd resonances can be excited; the most important one in the chosen range is just the $\nu_x = 7/3$ yet analysed before in phase space with the sextupolar field only. Switching on the decentralisation of the charge distribution (Fig. 9b), the third-integer resonance appears and because it is stronger than the $\nu_x = 9/4$ one, it becomes the higher peak in

the picture (the previous peak at 2.33 is enlarged up to 2.3333); two other odd non-linear resonances seems also to appear. Further simulations show that different odd resonances are excited with different displacements of the cylindrical charge distribution.

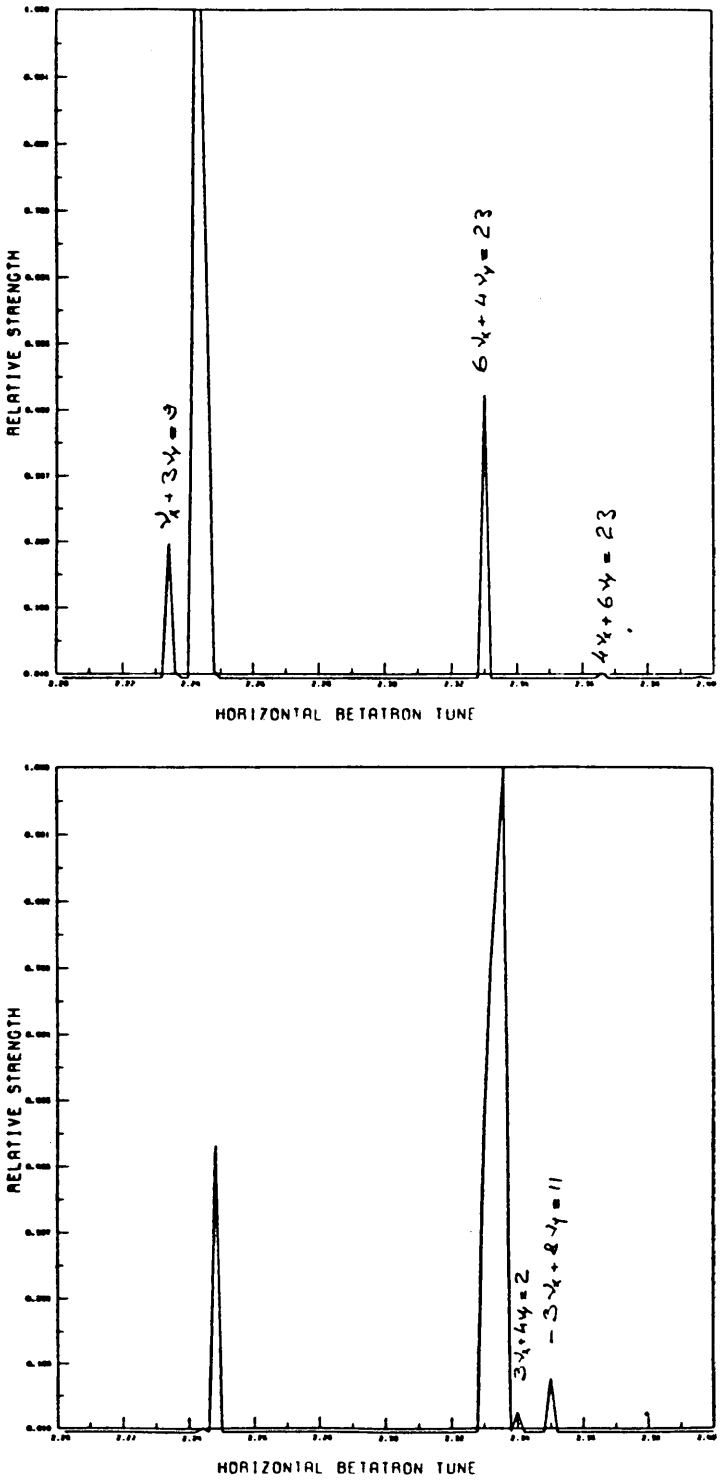

Fig. 9 - Some non-linear resonances simulated by means of a gaussian charge distribution ("cylindrical distribution"; $\sigma_x = \sigma_y$) with a definite even parity in (a) and a non-definite parity in (b).

Similar pictures obtained with the elliptical charge distribution are shown in Fig. 10. Again the coupling constant ξ used here is two orders of magnitude smaller than with the cylindrical distribution (Fig. 9). Two main resonances are reproduced by the elliptical distribution without decentralisation. With the elliptical charge distribution the force acting on the particle is not in radial direction but the same considerations on parity (even) apply as well because the charge distribution has still a definite even parity. Two main even resonances ($\nu_x = 9/4$, $\nu_x = 18/8$) are reproduced in Fig. 10a in which no decentralisation has been introduced. Switching on the decentralisation of the elliptical charge distribution the 3 main odd resonances in the range also appear ($\nu_x = 11/5$, $\nu_x = 7/3$, $\nu_x = 12/5$). Further peaks are present and their most probable identification is given in Fig. 10b. Again, as with the cylindrical distribution, different odd resonances seem to be excited by different decentralisation of the charge distribution.

The phase-space behaviour of the map near the third-integer resonance $\nu_x = 7/3$ with elliptical distribution of non-definite parity is shown in Fig. 11. Both pictures refer to four different initial amplitudes in $x\text{-}p_x$ plane and a fixed one in the $y\text{-}p_y$ plane. Motion with different initial amplitude in the $x\text{-}p_x$ plane has therefore quite the same behaviour in the $y\text{-}p_y$ plane; this can suggest that with the chosen ξ value the coupling between the two planes is still weak. Nevertheless, the chosen ξ value is great enough to show in the $x\text{-}p_x$ plane the characteristic behaviour of the third-integer resonance with rational and irrational tori.

In spite of the area filling property of the representative point in Fig. 11, the motion is only near a chaotic behaviour but still regular. Indeed, Fig. 12 shows the evolution of the distance in phase space of two representative points which are initially close together in the first diffuse region of Fig. 11 (near an irrational torus). With the same ξ value, as in Fig. 11, the motion seems still regular (linear increase of the distance). Increasing the coupling constant ξ only from 0.02 to 0.03 causes the onset of chaotic motion (Fig. 12b) with the exponential growth of the distance and the particle lost.

5. *CONCLUSIONS*

A direct map approach seems to be powerful in simulations of systems characterised by non-linear dynamics such as the one generated by the interaction of antiprotons with ions of residual gas (beam-beam-like interaction) in the CERN Antiproton Accumulator. The approach used here describes in a very simplified fashion the transverse betatron motion in storage rings (harmonic oscillations) and the attention is focused to the study of more interesting aspects of non-linear coupling perturbation between x and y degrees of freedom. Furthermore, the Mathieu approach on the map includes straightforward the tune modulation in a consistent way.

The high number of map iterations (in short computer times) which are possible because of the extremely simplified model of transverse betatron motion is perhaps the major advantage of a direct map method used here. In this way, we can study directly the phase-space structure and its evolution as some fundamental physical parameters such as betatron tunes and coupling constant of the interaction are modified. The high number of turns allows also a precise study of phase-space behaviour near very weak high-order resonances and their identification.

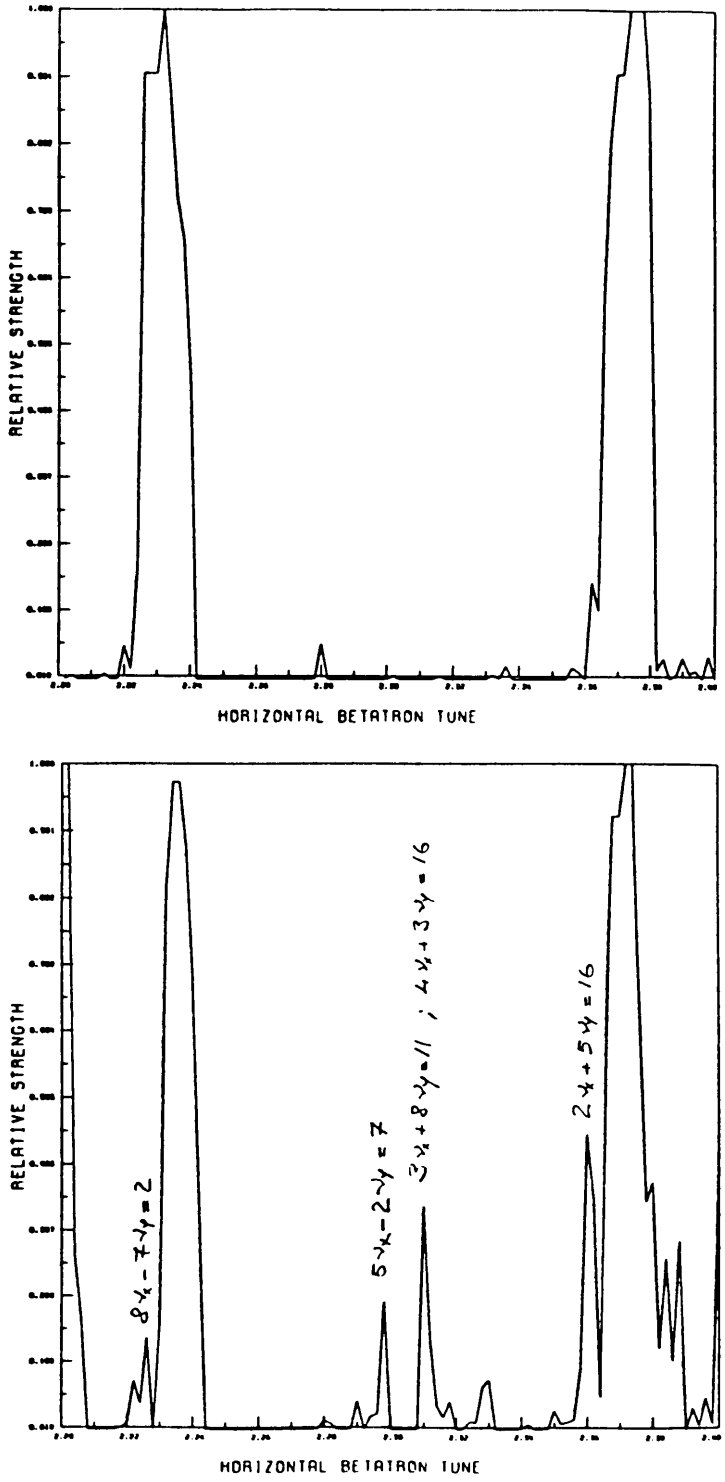

Fig. 10 - *Some non-linear resonances simulated by means of a gaussian charge distribution ("elliptical distribution"; $\sigma_x > \sigma_y$) with a definite even parity in (a) and a non-definite parity in (b).*

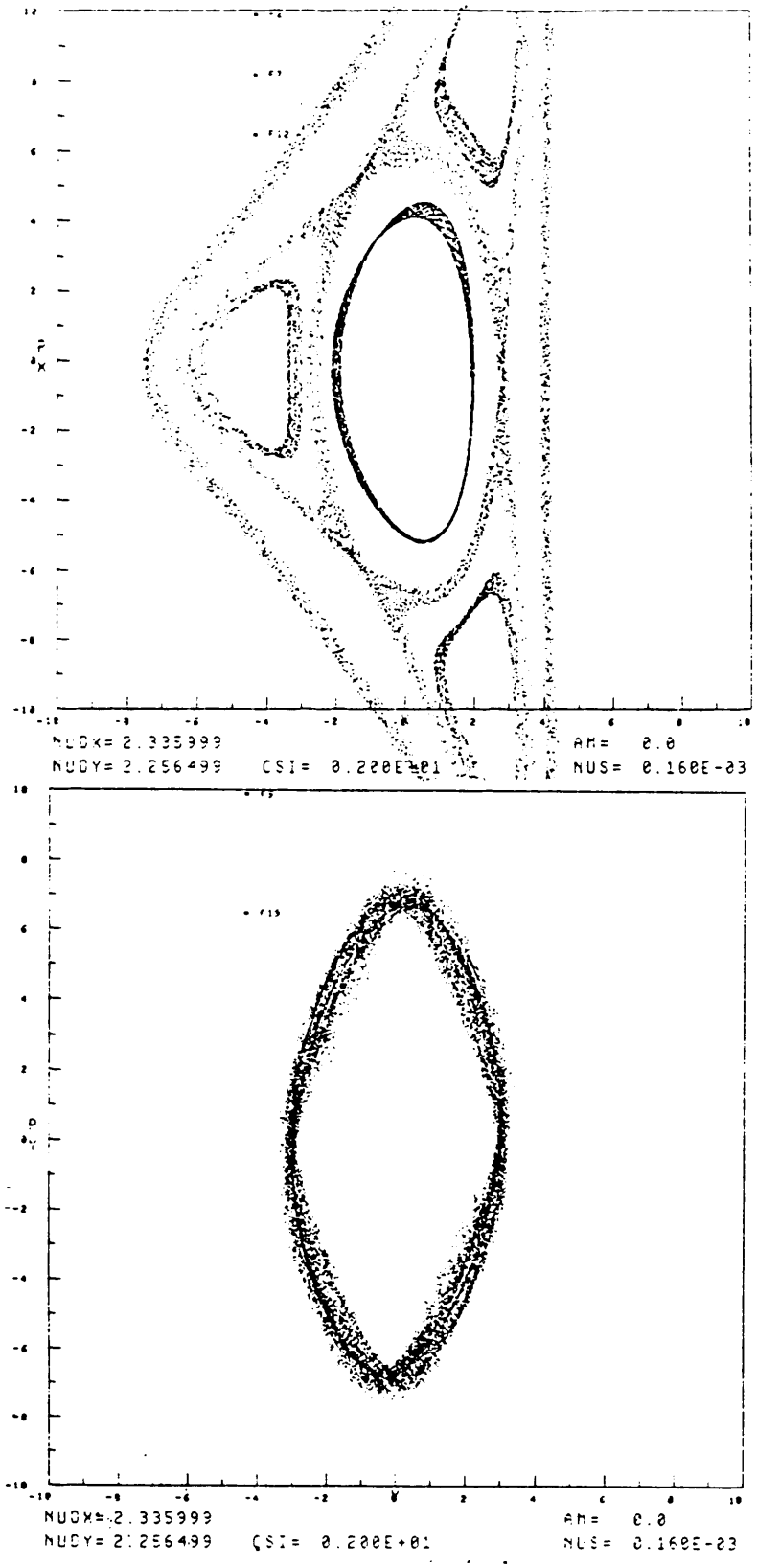

Fig. 11 - ***Phase space behaviour of the map with elliptical distribution and a non-definite parity near a third-integer resonance.***

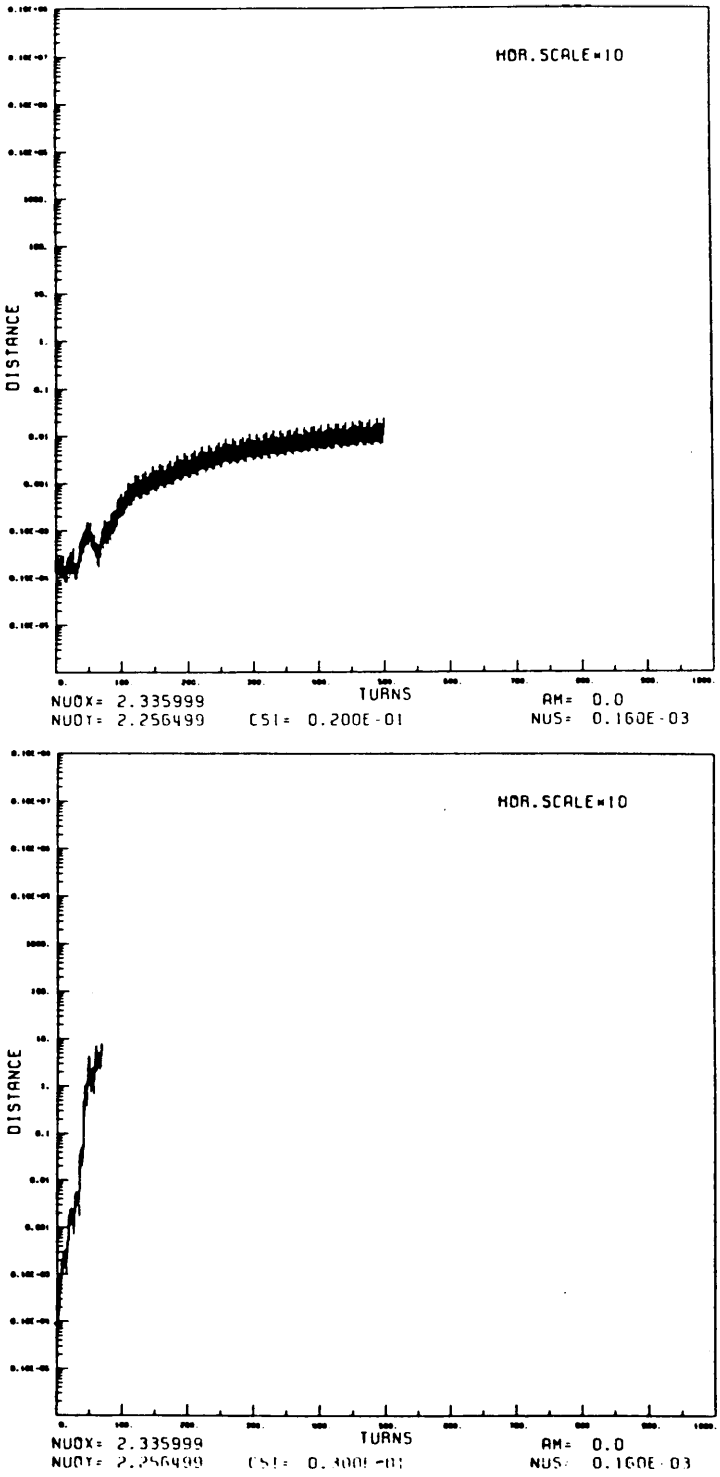

Fig. 12 - Evolution of the distance in phase space for two representative points initially close together; signature for regular (a) and chaotic (b) motion; note the ξ values.

The behaviour of the maps (or the motion of the particle) have been studies with different ion distributions (determined by the beam); from this study comes out the confirmation that charge distributions with gaussian shape and different standard deviations in x and y directions ("elliptical distribution"; $\sigma_x > \sigma_y$) are more effective than the cylindrical one ($\sigma_x = \sigma_y$) for the excitation of high-order non-linear resonances. Nevertheless, the first expected non-linear resonances are not all reproduced by the elliptical distribution; a more refined study can be useful with the choice of an elliptical distribution of ions truncated at $x_i = \sigma_i$; this distribution can have a more physical meaning because of the incomplete neutralisation of the beam. With this improvement it is possible that also the disagreement between the physical coupling and the numeric constants ($\varepsilon_{phys} = 10^{-1}\varepsilon_{num}$) can be solved.

ACKNOWLEDGEMENTS

I am very grateful to Dr. E.J.N. Wilson who first gave me hints for general study on transverse non-linear instabilities, in particular for their applications on antiproton-ion interactions in the CERN Antiproton Accumulator. I am also grateful to Dr. Wilson for all the time he dedicated to me for helpful discussions and useful suggestions.

I wish to thank Prof. M. Pusterla of the Università degli Studi di Padova (Dipartimento di Fisica) for many interesting discussions and his continuous guidance during all the work.

Furthermore, I would like to express here my thanks to Dr. F. Pedersen for his kind patience in focusing my attention on some experimental aspects of the CERN Antiproton Accumulator.

Finally, I owe special thanks to the Organization, in particular to the Antiproton Accumulator Group for their support and kind hospitality.

REFERENCES

1. E. Jones et al., Proc. Part. Acc. Conf. Vancouver, 1985, IEEE Trans. Nucl. Sci. NS-32, CERN/PS/85-15 (AA), 1985.

2. L.R. Evans, Proc. CERN Accelerator School (Antiprotons for Colliding Beam Facilities), Geneva, CERN 84-15, 319, 1984.

3. E.J.N. Wilson, CERN/83-10, 1983.

4. V.I. Arnold, "Mathematical Methods of Classical Mechanics", Springer-Verlag New York and Heidelberg, 1978.

5. E.D. Courant, R.D. Ruth, W.T. Weng, SLAC-PUB 3415, August 1984.

6. A. Pascolini and M. Pusterla, Particle Acc. 12, 121, 1982.

7. M. Pusterla, Private Communication.

8. G. Turchetti, Private Communication.

9. M. Bassetti and G.A. Erskine, CERN/ISR-TH/80-06, 1980.

10. M. Abramowitz and I.A. Stegun, Handbook of Math. Functions, National Bureau of Standards, Washington DC, 1966.

11. K.S. Kolbig, Complex Error Function, Program C 335, CERN, Geneva, 1970.

12. E.J.N. Wilson, Proc. of CERN Accelerator School (Advanced Accelerator Physics), Oxford UK, September 1985, CERN-PS/86-7 (AA), 1986.

13. A. Schoch, CERN 57-21, Geneva, February 1958.

14. A. Piwinsky, IEEE Trans. Nucl. Sci. NS-24, 1408, 1977.

15. A. Piwinsky, IEEE Trans. Nucl. Sci. NS-32, 2240, 1985.

16. H. Mais, F. Schmidt and A. Wrülich, Proc. Part. Acc. Conf. Vancouver, 1985, IEEE Trans. Nucl. Sci. NS-32, 2252, 1985.

17. R. Abraham, J.E. Marsden, "Foundation of Mechanics", The Benjamin Publ. Co. Inc., Reading MA (USA), 1978.

APPENDIX A

MATHIEU FUNCTIONS

If $q \ll 1$, the homogenous Mathieu equation

$$x''(z) + (a - 2q\cos 2z)x(z) = 0 \qquad (a.1)$$

has the following solutions (elliptical cosinus and elliptical sinus) [13]:

$$\begin{aligned} M(z,q) = {} & \cos\nu z - (1/4)\, q\, [(\cos(\nu+2)z)/(\nu+1) - (\cos(\nu-2)z)/(\nu-1)] \\ & + (1/32)q^2\, [(\cos(\nu+4)z)/(\nu+1)(\nu+2) + (\cos(\nu-4)z)/(\nu-1)(\nu-2)] - \\ & - (1/128)\, q^3\, [(\nu^2+4\nu+7)(\cos(\nu+2)z)/(\nu-1)(\nu+1)^3(\nu+2) - \\ & - (\nu^2-4\nu+7)(\cos(\nu-4)z)/(\nu+1)(\nu-1)^3(\nu-2) \\ & + (\cos(\nu+6)z)/3(\nu+1)(\nu+2)(\nu+3) - \\ & - (\cos(\nu-)z)/3(\nu-1)(\nu-2)(\nu-3)] + \ldots \end{aligned} \qquad (a.2)$$

$$\begin{aligned} N(z,q) = {} & \sin\nu z - (1/4)\, q\, [(\sin(\nu+2)z)/(\nu+1) - (\sin(\nu-2)z)/(\nu-1)] \\ & + (1/32)q^2\, [(\sin(\nu+4)z)/(\nu+1)(\nu+2) + (\sin(\nu-4)z)/(\nu-1)(\nu-2)] - \\ & - (1/128)\, q^3\, [(\nu^2+4\nu+7)(\sin(\nu+2)z)/(\nu-1)(\nu+1)^3(\nu+2) - \\ & - (\nu^2-4\nu+7)(\sin(\nu-4)z)/(\nu+1)(\nu-1)^3(\nu-2) \\ & + (\sin(\nu+6)z)/3(\nu+1)(\nu+2)(\nu+3) - \\ & - (\sin(\nu-)z)/3(\nu-1)(\nu-2)(\nu-3)] + \ldots \end{aligned} \qquad (a.3)$$

with $a = \nu^2 + q^2/2(\nu^2-1) + q^4(5\nu^2+7)/32(\nu^2-1)^3(\nu^2-4) + \ldots$ (a.4)

therefore if $q \ll 1$ we have $a \simeq \nu^2$.

If , as with the CERN AA parameters, the value of q is not less than unity ($q = 2\lambda(\nu_x/\nu_s)^2 \simeq 2\cdot 10^4$ for the AA) still an approximate analytical solution can be obtained by means of the Liouville transform [8]:

$$\zeta = \int_0^z \sqrt{(a - 2q\cos 2z')}\, dz' \qquad (a.5)$$

$$x = \eta \,/\, (\sqrt[4]{(a - 2q\cos 2z)}) \qquad (a.6)$$

neglecting terms of the order of $(2q/a)^2$ we obtain a new Mathieu equation in terms of the η variable with solutions which are valid when $q \gg 1$:

$$M_L(z) = (a - 2q\cos 2z^*)M(z^*) \qquad (a.7)$$

$$N_L(z) = (a - 2q\cos 2z^*)N(z^*) \qquad (a.8)$$

where M(z) and N(z) are again the elliptical cosinus and elliptical sinus given in expressions (a.2) and (a.3) evaluated at

$$z^* \simeq z - (q/2a)\sin 2z - \ldots \qquad \text{(a.9)}.$$

* * *